Electrical Transport and Thermoelectric Properties of Cr-doped Monolayer MoS_2 and WS_2 via Density Functional Theory and Boltzmann Transport Simulation

Chieh-Yang Chen[1,2] and Yiming Li[1-4,*]

[1]Parallel and Scientific Computing Laboratory; [2]Institute of Communications Engineering; [3]Institute of Biomedical Engineering; [4]Department of Electrical and Computer Engineering, National Yang Ming Chiao Tung University, 1001 Ta-Hsueh Rd., Hsinchu 300, Taiwan, *Tel: +886-3-5712121 ext. 52974; Fax: +886-3-5726639; Email: ymli@faculty.nctu.edu.tw

***Abstract*—This work computationally studies the monolayer (ML) MoS_2, WS_2 and the substitutional Cr-doped ones. The lattice parameters, band structure, density of state are calculated from the density functional theory (DFT). The electron mobility and Seebeck coefficient are estimated from the linearized Boltzmann transport equation (BTE). Compared with ML-MoS_2 and ML-WS_2, the direct band gaps of Cr-doped ML-MoS_2 and ML-WS_2 are reduced via DFT calculation. For the Cr-doped ML-MoS_2 and ML-WS_2, estimated by the linearized BTE, the values of electron mobility are about 5.7 and 11.8 times variations when the doping concentration increase from 10^8 to 10^{12} cm^{-2} at room temperature. The magnitudes of electron Seebeck coefficient of Cr-doped ML-MoS_2 and ML-WS_2 are about 1220 and 1210 μV/K at the doping concentration of 10^8 cm^{-2}.**

Keywords—Molybdenum disulfide; Tungsten disulfide; Transition metal doping; Substitutional doping; Boltzmann transport equation; Mobility; Thermoelectric.

I. Introduction

The transition-metal dichalcogenide (TMD) in the two-dimensional material family has drawn many attentions owing to its direct band gap of monolayer structure and great process stability. The researchers seek the ways to modify the material properties such as doping techniques by using the first-principle-theory [1-2]. At the same time, the electronic transport and thermoelectric properties of pure monolayer MoS_2 (ML-MoS_2) and other two-dimensional materials are revealed via BTE [3-4] in recent years. The BTE studies can estimate the transport properties of a material with n- or p-type doping. However, these studies focus on the pure materials or only properties for electron.

In this work, not only pure monolayer MoS_2 and WS_2 but also transition-metal-doped ones are discussed. First, to examine the model of this work, the carrier mobility of monolayer MoS_2 and WS_2 are considered as the benchmark due to its abundent experimental and theoretical literatures. Since the experimental works so far are mainly based on fabricated transistors with pure MoS_2 or WS_2, those measurement can be considered as intrinsic device parameters; thus, our results of BTE with low doping concnetration will be compared with these results. Then, based on this technique, we can estimate the intrinsic properties of semiconductor materials by the linearized BTE by setting low doping concentration. From the simulated band structure, we find out the Cr-doped ML-MoS_2 and ML-WS_2 still possess semiconductor properties with the direct band gaps. We do further study the carrier mobility and Seebeck coefficient of these Cr-doped materials.

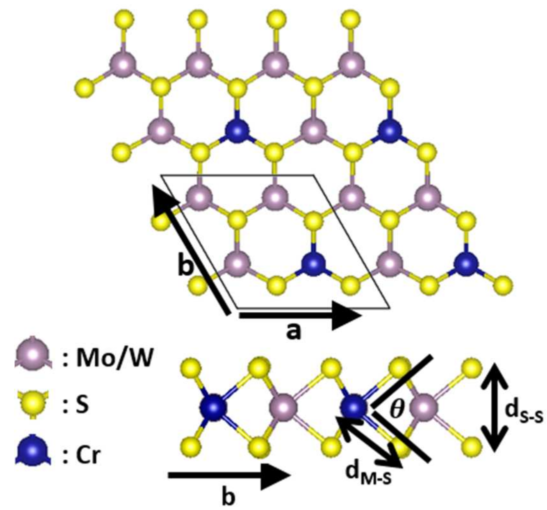

Fig. 1. The lattice structure of Cr-doped monolayer MS_2 (M = Mo, W) One of the Mo or W atom is replaced by Cr atom in a 2 × 2 monolayer MoS_2 or WS_2 supercell and the structures are denoted as Mo_3S_8Cr and W_3S_8Cr, respectively.

II. The Simulation Methodology

The structure relaxation and electronic band structure are calculated via using Vienna ab initio Simulation Package (VASP) [5] under spin-polarized density functional theory (DFT). The approach of Perdew-Burke-Ernzerhof (PBE) is used as the exchange-correlation function in this study, the accuracy are examined in our earlier work [6-7]. The cutoff kinetic energy is 500 eV which is tested for accuracy for bulk and monolayer structures. The Brillouin zone (BZ) was sampled with 18 × 18 × 1 and 10 × 10 × 1 Γ-centered *k*-meshes under the Monkhorst–Pack scheme [6-7] for pure and Cr-doped structures, respectively. The force acting on each atom of relaxed structure is smaller than 5×10^{-4} eV/Å; the energy difference is less than 10^{-8} per atom. A 15 Å-thick vacuum layer is applied along c axis to decouple the periodic images between adjacent monolayers. Figure 1 shows the Cr-doped monolayer MoS_2 and WS_2

The process of density function theory (DFT) + Boltzmann transport equation (BTE)

Step 1: Structure relaxation

Step 2: Deformation potential:
- **Generate deformed structures**
- **Calculate deformation potential**

Step 3: Elastic properties calculation
- **Use strain-stress relation**

Step 4: Dielectric properties calculation:
- **Use perturbation theory**

Step 5: BTE
- **Define scattering types**
- **Define temperature and doping range**
- **Load values of deformation potential, elastic properties, and dielectric properties**
- **Electron mobility and Seebeck coefficient are calculated using the linearized BTE via the Onsager transport coefficients**

Fig. 2. The steps of simulation are mainly based on the density functional theory and Boltzmann transport equation. First, an atomic structure is relaxed via VASP with strict convergence. Then, according to this result, the deformation potential, elastic coefficients, and the dielectric coefficients are calculated sequentially. The deformation potential is calculated by the energy of generated deformed and un-deformed structures. The elastic constants are determined by the strain-stress relationship. The calculation of dielectric constants is using the perturbation theory in VASP. Then, Born effective charges, piezoelectric constants, and ionic contributions to the dielectric tensor can be calculated accordingly. With these values, the linearized Boltzmann transport is solved and the electronic transport and thermoelectric properties are obtained [15, 16, 17].

TABLE I. LIST OF THE SIMULATED LATTICE PARAMETERS AMONG THE STUDIED STRUCTURES

	ML-MoS_2	ML-WS_2	Mo_3S_8Cr	W_3S_8Cr
a (Å)	3.18	3.181	6.299	6.307
$d_{M\text{-}S}$ (Å)	2.413	2.419	2.329	2.338
$d_{S\text{-}S}$ (Å)	3.131	3.148	3.169	3.169
θ (deg)	80.9	81.185	81.983	82.086
E_g (eV)	1.693	1.838	1.291	1.288

(denoted as Mo_3S_8Cr and W_3S_8Cr) built from 2 × 2 × 1 monolayer MoS_2 and WS_2 supercells with one Mo or W atom replaced by Cr atom. Figure 2 indicates the key steps from DFT simulation to BTE calculation of this work. The acoustic deformation potential scattering (ADP) and ionized impurity scattering (IMP) are included for studying the electrical and thermoelectric transport properties. The values of deformation potential and elastic constant are for ADP scattering; the values of dielectric constant are for IMP scattering. These aforementioned values are separately simulated and extracted from VASP results under the relaxed structure. The cutoff kinetic energy for simulation of elastic properties is 550 eV for ML-MoS_2, ML-WS_2, and Cr-doped ones after a large range of convergence and stability tests. Not shown here, the simulated elastic tensor and dielectric coefficients are examined with the experimental works. Then, the BTE uses the grid uniformly interpolated into a dense mesh of 180 × 180 × 1 and 100 × 100 × 1 for undoped and Cr-doped structures, respectively. Our simulated electron mobilty of intrinsic MoS_2 is 52.4 $cm^2V^{-1}s^{-1}$

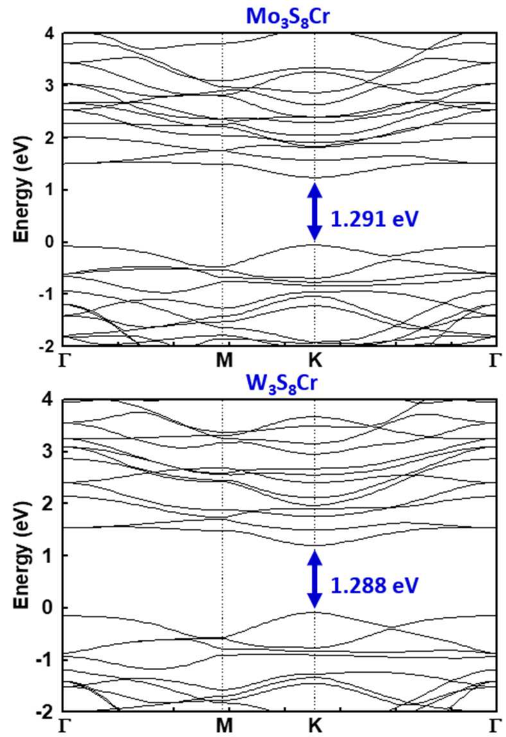

Fig. 3. The band structure of Mo_3S_8Cr and W_3S_8Cr. The simulated band structures of monolayer MoS_2, WS_2, Mo_3S_8Cr, and W_3S_8Cr show the direct band gap at K point of the BZ with values, 1.693, 1.838, 1.291, and 1.288 eV, respectively.

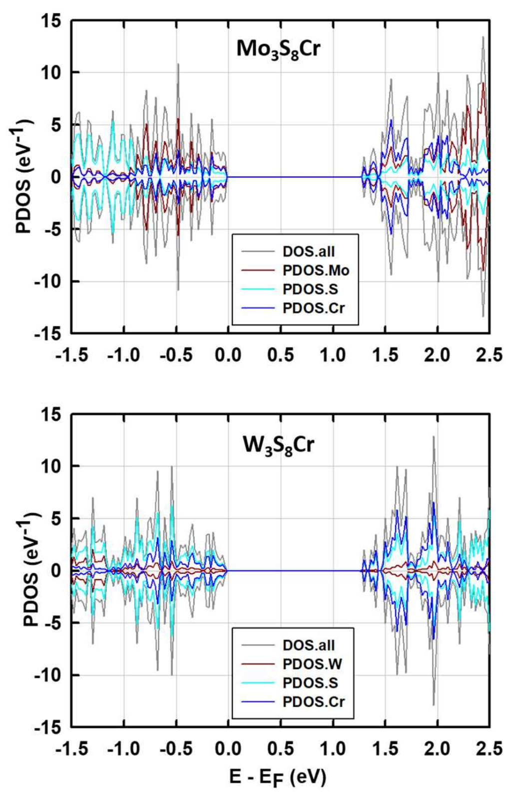

Fig. 4. The projected density of states (PDOS) of Mo_3S_8Cr and W_3S_8Cr with respect to each element. The Cr atom contributes additional states near the valence and conduction bands and reduces the band gap.

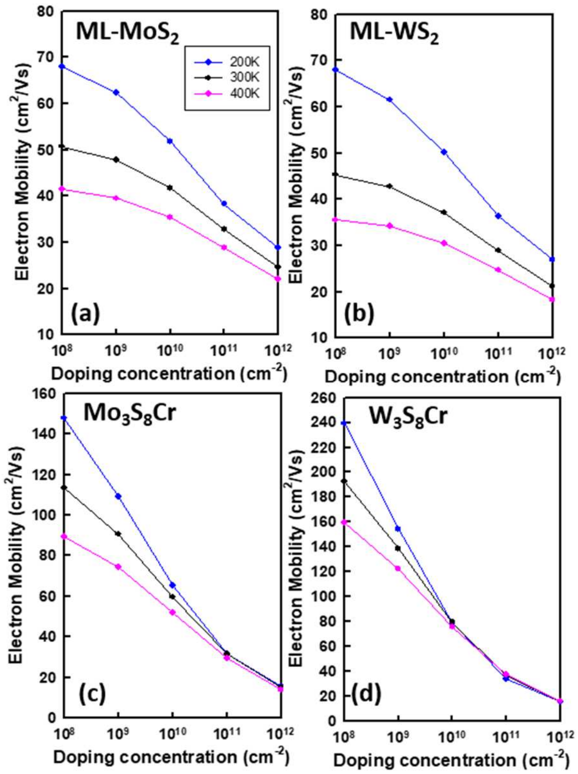

Fig. 5. The electron mobility of (a) monolayer MoS_2, (b) monolayer WS_2, (c) Mo_3S_8Cr, and (d) W_3S_8Cr for the doping concentration from 10^8 to 10^{12} cm^{-2}. The electron mobility decreases while the doping concentration increases mainly due to high impurity scattering. And, the mobility decreases at high temperature. (c)-(d) The Mo_3S_8Cr and W_3S_8Cr show the significant increase of electron mobility mainly because of their relatively reduced band gaps.

TABLE II. A Summarized Table of Averaged Electron Mobility with Low Doping Concentration. The Values of Electron of Monolayer MoS_2 and WS_2 with Low Concentration are Used to Compare with the Intrinsic Mobility from Other Experimental and Theoretical Works.

<table>
<tr><td></td><td colspan="4">Electron mobility (cm^{2}V^{-1}s^{-1}) of ML-MoS_2</td></tr>
<tr><td>Temperature</td><td>200 K</td><td>260 K</td><td>300 K</td><td>400 K</td></tr>
<tr><td>This work</td><td>71.7</td><td>60</td><td>52.4</td><td>42.4</td></tr>
<tr><td>Experimental [8]</td><td>-</td><td>-</td><td>37</td><td>-</td></tr>
<tr><td>Experimental [9]</td><td>-</td><td>-</td><td>80</td><td>-</td></tr>
<tr><td>Experimental [10]</td><td>-</td><td>-</td><td>40</td><td>-</td></tr>
<tr><td>Theorical [3]</td><td>-</td><td>-</td><td>47-68</td><td>-</td></tr>
<tr><td>Experimental [11]</td><td>-</td><td>64</td><td>-</td><td>-</td></tr>
<tr><td></td><td colspan="4">Electron mobility (cm^{2}V^{-1}s^{-1}) of ML-WS_2</td></tr>
<tr><td>Temperature</td><td>200 K</td><td colspan="2">300 K</td><td>400 K</td></tr>
<tr><td>This work</td><td>73.3</td><td colspan="2">47.6</td><td>37.2</td></tr>
<tr><td>Experimental [13]</td><td>-</td><td colspan="2">44</td><td>-</td></tr>
<tr><td>Experimental [14]</td><td>-</td><td colspan="2">50±7</td><td>-</td></tr>
<tr><td></td><td colspan="4">Electron mobility (cm^{2}V^{-1}s^{-1}) of ML-Mo_3S_8Cr</td></tr>
<tr><td>Temperature</td><td>200 K</td><td colspan="2">300 K</td><td>400 K</td></tr>
<tr><td>This work</td><td>189.6</td><td colspan="2">133.1</td><td>100.4</td></tr>
<tr><td></td><td colspan="4">Electron mobility (cm^{2}V^{-1}s^{-1}) of ML-W_3S_8Cr</td></tr>
<tr><td>Temperature</td><td>200 K</td><td colspan="2">300 K</td><td>400 K</td></tr>
<tr><td>This work</td><td>363.5</td><td colspan="2">251.9</td><td>194</td></tr>
</table>

which is in the range of 37-80 cm^{2}V^{-1}s^{-1} from various fabricated devices [8-10] and also falls in the range of 47-68 cm^{2}V^{-1}s^{-1} by other theoretical calculations [3]. For accuracy comparison, our simulated electron mobility at 260 K is close to the experimental value of 64 cm^{2}V^{-1}s^{-1} [11]. The Seebeck coefficient of electron of MoS_2 is 574 μV/K which is close to the theoretical value of 570 μV/K [14] with the doping concentration of 10^{11} cm^{-2} at the room temperature. For the intrinsic monolayer WS_2, our simulated electron mobility is 47.6 cm^{2}V^{-1}s^{-1} which is close to experimental works of 44 and 50±7 cm^{2}V^{-1}s^{-1} [13-14]. The definition of the doping concentration is based on the view of two-dimensional material; notably, the doping concentration of bulk material can be scaled by $dop_{2D} = dop_{3D} \times c$, where c is the length of simulated domain along the c-direction.

III. Results and Discussion

The lattice parameters of relaxed structures of this work are listed in Table I. The two distances, $d_{M\text{-}S}$ and $d_{S\text{-}S}$, are the distances from Mo/W atom to their neighbor S atom and from top S to bottom S atom, respectively. For Mo_3S_8Cr and W_3S_8Cr, the $d_{M\text{-}S}$ and $d_{S\text{-}S}$ are the distances from Cr atom to its neighbor S atom. Notably, the largest value of $d_{S\text{-}S}$ is chosen since it varies in Cr-doped structure. The simulated energy band structures are shown in the figure 3. Since the Cr, Mo, and W elements are all in VIB group of periodic table, the Cr-doped monolayer MoS_2 and WS_2 can remain direct band gap at K point of the BZ. The monolayer MoS_2, WS_2, Mo_3S_8Cr, and W_3S_8Cr show direct band gap at K point of the BZ with values, 1.693, 1.838, 1.291, and 1.288 eV, respectively. The projected density of states (PDOS) of Mo_3S_8Cr and W_3S_8Cr, as shown in the figure 4, indicate that the Cr atom contributes additional states near the valance and conduction bands and thus decreases the band gap significantly. Figures 5(a)-(d) plot the averaged electron mobility including ADP and IMP scattering for monolayer MoS_2, monolayer WS_2, Mo_3S_8Cr, and W_3S_8Cr with respect to different carrier concentrations from 10^8 to 10^{12} cm^{-2} and temperatures (T = 200, 300, and 400 K). The trend shows that the averaged electron mobility increases while the temperature decreases or the doping concentration decreases. Not shown here, the temperature effect and the doping concentration dominate the ADP and IMP scatterings, respectively. Compared with ML-MoS_2 and ML-WS_2, at the low doping concentration of 10^8 cm^{-2}, the Mo_3S_8Cr, and W_3S_8Cr have significantly higher electron mobility and adjustable range when temperature varies from 200 to 400 K. However, at the high doping concentration of 10^{12} cm^{-2}, the Mo_3S_8Cr, and W_3S_8Cr have marginal tunable ranges due to their relatively small band gaps.

The table II summarizes the values of averaged electron mobility of this work and other referenced works. The values of our work are from the BTE estimation with low doping

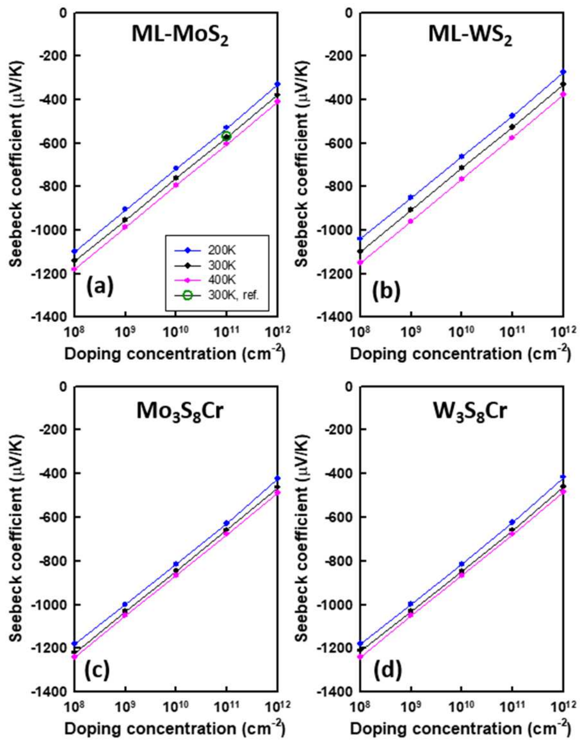

Fig. 6. (a)-(d) The Seebeck coefficient of electron respect to different carrier concentrations and temperatures for monolayer MoS_2, WS_2, Mo_3S_8Cr, and W_3S_8Cr. The Seebeck coefficient of electron of monolayer MoS_2 is 574 μV/K which is close to theoretical value of 570 μV/K [14] at concentration = 10^{11} cm^{-2} at room temperature. The result shows wide adjustable range. The absolute values of the electron Seebeck coefficient of the Mo_3S_8Cr and W_3S_8Cr are larger than those of the pure MoS_2 and WS_2.

concentration. These values indicate the possible maximum mobility among the studied structures of this work. The electron mobility of Mo_3S_8Cr, and W_3S_8Cr are about 2.54 and 5.29 times of ML-MoS_2 and ML-WS_2 at the room temperature, respectively. Not shown here, we also estimate the hole mobility. The hole mobility of Mo_3S_8Cr, and W_3S_8Cr are about 1.8 and 2.0 times of ML-MoS_2 and ML-WS_2 at the room temperature. The values of estimated Seebeck coefficient with respect to different doping concentrations and temperatures for monolayer MoS_2, WS_2, Mo_3S_8Cr, and W_3S_8Cr are plot in the figure 6. The absolute value of electron Seebeck coefficient is increased with the temperature at the same doping concentration and is decreased with the doping concentration under the same temperature.

IV. Conclusions

In summary, the electronic and thermoelectric transport properties of ML-MoS_2, ML-WS_2, and ML-Cr-doped ones have been explored by using DFT and BTE. The Cr-doped monolayer MoS_2 and WS_2 reserve their direct band gap property; however, their magnitudes are tunable via different doping concentration and doping species, not shown here. Compared with original ML-MoS_2 and ML-WS_2, for the averaged electron mobility, the ML-Mo_3S_8Cr, and ML-W_3S_8Cr have boosted ones (about 2.54 and 5.29 times at room temperature). The Seebeck coefficient of electron shows a wide adjustable numeric range with the varied doping concentration; and, notably, it is insensitivity to the temperature variation for all the studied structures.

Acknowledgment

This work was supported in part by the Ministry of Science and Technology, Taiwan, under Grant MOST 110-2221-E-A49-139, Grant MOST 109-2221-E-009-033, and Grant MOST 109-2634-F-009-030, and in part by the "Center for mm Wave Smart Radar Systems and Technologies" under the Featured Areas Research Center Program within the framework of the Higher Education Sprout Project by the Ministry of Education in Taiwan.

References

[1] C. Huang, Y. Jin, W. Wang, L. Tang, C. Song, and F. Xiu, "Manganese and chromium doping in atomically thin MoS_2," *J. Semicond.*, vol. 38, no. 3, p. 033004, 2017.

[2] E. Z. Xu, H. M. Liu, K. Park *et al.*, "p-Type transition-metal doping of large-area MoS_2 thin films grown by chemical vapor deposition," *Nanoscale*, vol. 9, no. 10, pp. 3576–3584, 2017.

[3] Y. Zhao, Z. Dai, C. Zhang *et al.*, "Intrinsic electronic transport and thermoelectric power factor in n-type doped monolayer MoS_2," *New J. Phys.*, vol. 20, no. 4, p. 43009, 2018.

[4] Z. Gao and J.-S. Wang, "Thermoelectric Penta-Silicene with a High Room-Temperature Figure of Merit," *ACS Appl. Mater. Interfaces*, vol. 12, no. 12, pp. 14298–14307, Mar. 2020.

[5] G. Kresse and J. Hafner, "Ab initio molecular dynamics for liquid metals," *Phys. Rev. B*, vol. 47, no. 1, pp. 558–561, 1993.

[6] Y. Tsai and Y. Li, "On electronic structure and geometry of MoX_2 (X = S, Se, Te) and black phosphorus by ab initio Simulation with various van der Waals corrections," in *International Conference on Simulation of Semiconductor Processes and Devices* (*SISPAD*), 2017, pp. 169–172.

[7] C. Y. Chen and Y. Li, "Numerical calculation of electronic properties of transition metal-doped mWS_2 via DFT, " in M. van Beurden, N. V. Budko, and W. Schilders (Eds.), Scientific Computing in Electrical Engineering SCEE 2020, Springer Nature Switzerland AG, ISBN: 978-3-030-84237-6, 2021, pp. 49-56.

[8] K. Hippalgaonkar, Y. Wang, Y. Ye *et al.*, "High thermoelectric power factor in two-dimensional crystals of MoS_2," *Phys. Rev. B*, vol. 95, no. 11, p. 115407, 2017.

[9] H. S. Lee, S.-W. Min, Y.-G. Chang *et al.*, "MoS_2 Nanosheet Phototransistors with Thickness-Modulated Optical Energy Gap," *Nano Lett.*, vol. 12, no. 7, pp. 3695–3700, Jul. 2012.

[10] J. Zhao, N. Li, H. Yu *et al.*, "Highly Sensitive MoS_2 Humidity Sensors Array for Noncontact Sensation," *Adv. Mater.*, vol. 29, no. 34, p. 1702076, 2017.

[11] B. Radisavljevic and A. Kis, "Mobility engineering and a metal–insulator transition in monolayer MoS_2," *Nat. Mater.*, vol. 12, no. 9, pp. 815–820, 2013.

[12] S. Kim, C. Lee, Y. S. Lim, and J.-H. Shim, "Investigation for Thermoelectric Properties of the MoS_2 Monolayer–Graphene Heterostructure: Density Functional Theory Calculations and Electrical Transport Measurements," *ACS Omega*, vol. 6, no. 1, pp. 278–283, Jan. 2021.

[13] S. Jo, N. Ubrig, H. Berger, A. B.Kuzmenko, and A. F. Morpurgo, "Mono- and Bilayer WS_2 Light-Emitting Transistors," *Nano Lett.*, vol. 14, no. 4, pp. 2019–2025, Apr. 2014.

[14] D. Ovchinnikov, A. Allain, Y.-S. Huang, D. Dumcenco, and A. Kis, "Electrical Transport Properties of Single-Layer WS_2," *ACS Nano*, vol. 8, no. 8, pp. 8174–8181, Aug. 2014.

[15] G. K. Madsen, J. Carrete, and M. J. Verstraete, "BoltzTraP2, a program for interpolating band structures and calculating semi-classical transport coefficients." *Comput. Phys. Commun.*, vol. 231, pp. 140-145, 2018.

[16] L. Onsager, "Reciprocal relations in irreversible processes I," *Phys. Rev.*, vol. 37, pp. 405-426, Feb. 1931.

[17] A. M. Ganose, J. Park, A. Faghaninia, R. Woods-Robinson, K. A. Persson, and A. Jain, "Efficient calculation of carrier scattering rates from first principles," *Nat. Commun.*, vol. 12, p. 2222, 2021.